forests

MDPI

Article

Effects of Dowel Rotation Welding Conditions on Connection Performance for Chinese Fir Dimension Lumbers

Xiao Zhong [1,†], De Li [1,†], Xiaoxue Xu [1], Quan Li [2], Danyun Yu [1], Zhigang Wu [1,3,*], Jiankun Liang [3,4,*], Jun Peng [5], Wen Gu [1], Xin Zhao [1], Shuang Yin [1], Guifen Yang [1] and Feiyan Gong [1]

[1] College of Forestry, Guizhou University, Guiyang 550025, China; 18985361700@163.com (X.Z.); lide228@163.com (D.L.); x3402691660@163.com (X.X.); 13511964266@163.com (D.Y.); gwen490929@163.com (W.G.); zx3347559@163.com (X.Z.); yinshuang824@163.com (S.Y.); 15772783270@163.com (G.Y.); 15285111783@163.com (F.G.)
[2] College of Civil Engineering and Architecture, Suqian University, Suqian 223800, China; liquan-8@163.com
[3] College of Civil Engineering, Kaili University, Kaili 556011, China
[4] International Joint Research Center for Biomass Materials, Southwest Forestry University, Kunming 650224, China
[5] College of Mechanics, Guizhou University, Guiyang 550025, China; 19110747083@163.com
* Correspondence: wzhigang9@163.com (Z.W.); dushimensheng@126.com (J.L.); Tel.: +86-851-8829-8397 (Z.W.)
† These authors contributed equally to this work.

Abstract: In this study, the rotating welding process of Chinese fir (*Keteleeriafortunei*) in Guizhou, China, was systematically analyzed. The effects of rotating welding conditions, including the dowel-to-guide hole diameter ratio, welding time, depth, base surface, angle, and dowel type, on the performance of welded Chinese fir were explored. Moreover, the physical and chemical changes oftheChinese fir interface during welding were revealed by Fourier-Transform Infrared Spectroscopy (FT-IR), X-ray Photoelectron Spectroscopy (XPS), X-ray Diffraction (XRD), and Scanning Electron Microscopy (SEM). The results indicated the following: (1) The rotating welding technology can quickly achieve a strong connection between wood through friction heat without chemical adhesives and compared with traditional wood connection technology such as gluing or mechanical fixing;it has the advantages of simple operation, high production efficiency; and environmental friendliness. (2) Aftertherotating welding, the wood underwent significant pyrolysis, especially the degradation of hemicellulose. The heat generated in the welding process caused good melting and mechanical interlocking between the dowel and the wall of the guide hole, but it was also accompanied by afriction loss of the dowel and the substrate. (3) The welding parameters affected the wood's connection strength and stability by altering heat production, distribution, transfer, and frictional losses. The impact of the dowel-to-guide hole diameter ratio had a great influence on the connection strength. When the diameter ratio was 1:0.7, the tensile strength was the highest, reaching 2.27 MPa. (4) The analyses of XPS, FTIR, XRD, and SEM proved thatthechemical composition changes at the interface, leading to a more structured crystalline bond and enhanced connection strength due to fiber entanglement and interlocking. This research providesatheoretical and experimental basis forthefurther innovation and development of wood processing technology and provides a new technical path forthegreen manufacturing of wood structure buildings.

Keywords: Chinese fir dimension lumber; rotational welding; welding parameters; heat generation; heat transfer; wood degradation

Citation: Zhong, X.; Li, D.; Xu, X.; Li, Q.; Yu, D.; Wu, Z.; Liang, J.; Peng, J.; Gu, W.; Zhao, X.; et al. Effects of Dowel Rotation Welding Conditions on Connection Performance for Chinese Fir Dimension Lumbers. *Forests* **2024**, *15*, 1038. https://doi.org/10.3390/f15061038

Academic Editor: Christian Brischke

Received: 3 June 2024
Revised: 11 June 2024
Accepted: 12 June 2024
Published: 15 June 2024

1. Introduction

Because of its excellent insulation, environmental protection, energy saving, and safety, wood structure buildings have been widely recognized and promoted around the world. As a country rich in forestry resources, Chinese fir has been widely used in the furniture and construction industries due to its lightweight and easy processing [1–7]. Especially in the

Guizhou Province, Chinese fir is not only the main economic forest species but is also the main building material of traditional wooden dwellings with national characteristics [8–10]. According to statistics, Chinese fir occupies an important share ofChina's forest resources, and its annual growth rate and cutting amount are at the forefront, indicating its core position in the domestic forestry industry [11–15].

Traditional furniture and architectural joints, like mortise and tenon, round dowel joints, metal connectors, and glue joints, while prevalent, face challenges like complex production processes, significant wood loss, metal corrosion, and low efficiency [16–21]. In order to solve these problems, wood welding technology, as an emerging environmentally friendly and efficient connection technology, has attracted the attention of researchers and industry [22–26]. Since wood welding technology was first proposed by Suthoff [27], it has experienced the development of various technologies from linear friction welding to rotary friction welding, ultrasonic wood welding, and laser wood welding [22,28–31].

Rotary friction welding is regarded as an important innovation in wood joining technology because of its instantaneous bonding characteristics and superior environmental performance [32–35]. The rotary friction welding technology softens the lignin through the friction heat generated by the contact of the high-speed rotating wood tenon with the wood substrate, thereby enabling rapid bonding of the wood without the need for any adhesive. This technology not only improves the fastness and durability of the connection but also significantly improves the production efficiency, which is an ideal choice for industrial large-scale production [36–44]. In recent years, with the increasingly strict environmental regulations and the continuous growth of wood construction demand, the research and application of rotary friction welding technology have been greatly promoted.

In this study, the application potential of rotary welding technology in the connection of Chinese fir and the influence of process parameters on the connection performance were explored, aiming to provide theoretical and practical support for the wider application of Chinese fir and the green manufacturing of wood structure buildings.

2. Materials and Methods

2.1. Materials

Chinese fir (*Keteleeriafortunei*) wood, which is a common forest resource with a solid structure and interleaving fiber, is suitable for wood construction and furniture manufacturing. Chinese fir in Guizhou is chosen as the research object because it has a wide planting area and important economic value in the local area. The Chinese fir is produced in the Pingba District near Anshun, Guiyang, China, with a geographical position of 106.43° E and 26.34° N. The Chinese fir wood is approximately 25 years old, with an average air-dry density of 0.42 g/cm^3 and a moisture content of 12%. The dowels employed include the Schima superba with an average air-dry density of 0.67 g/cm^3, Beech with 0.64 g/cm^3, and Eucalyptus with 0.73 g/cm^3, all bought from the market and maintaining an average moisture content of 12%.

2.2. Pretreatment of Chinese Fir Dimension Lumbers

The samples of Chinese fir dimension lumber that met the standards were selected, and the surface was cleaned and dried to ensure that the surface of the samples was clean and smooth. Then, the sample was cut into a standard size of 50 mm (length) × 40 mm (width) × 30 mm (thickness), in order to ensure the repeatability and comparison of the experiment.The sampling areas on the cross-section or length of the Chinese fir logs were accurately measured and marked using professional measuring tools. Appropriate sawing or cutting tools were employed to cut along the marked lines in order to extract the target samples. The obtained samples underwent proper processing, which involved smoothing the surfaces, removing sawdust, and marking the sample information, to prepare them for subsequent testing or analysis. Depending on the requirements, the processed samples were appropriately packaged and preserved to protect against environmental factors such as humidity, temperature, and light exposure.

2.3. Welding Parameters Setting

According to the pre-test results, a series of specific parameters were adopted to ensure the stability and comparability of the welding effect, as shown in Table 1.

Table 1. Welding process parameter setting.

Parameters	Set Value
Diameter ratio of dowel to guide hole	1:0.9, 1:0.8, 1:0.7
Standing time of welding	0 s, 1 s, 2 s
Welding depth	15 mm, 20 mm, 25 mm
Welding surface	Cross section, radial section, and tangential section
Welding angle	30°, 45°, 60°, 90°
Dowel type	Schima superb, Beech, Eucalyptus

2.4. Preparation of Welded Chinese Fir Dimension Lumbers and the Test

Chinese fir specimens were conditioned under constant temperature and humidity with good ventilation for six months to stabilize their moisture content at approximately 12%. Samples free of knots, cracks, decay, and discoloration were selected as the base material for welding. As shown in Figure 1, a ProxxonTyp 28 21 drill press (Proxxon, Stuttgart, Germany) was used to drill guide holes in the radial plane of the fir base material, with a speed of 2400 rpm, hole diameter of 8 mm, and depth of 20 mm. The dowels were then fixed to the drill press, aligned with the center of the guide holes, and rotationally welded at the same speed to a depth of 20 mm. According to the literatures [45–47], a WDS-50KN universal testing machine was used at a uniform loading speed of 2.5 mm/min to test the tensile strength of the rotational welding joints. Stress–strain curves were recorded for mechanical analysis, with the final tensile pull-out strength being the average of 24 specimens. The maximum and minimum values were deleted, and then the rest of the samples were averaged. The standard deviation was less than 5%.

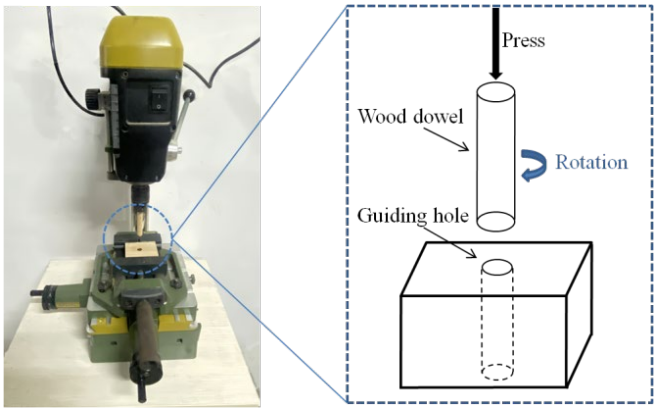

Figure 1. Diagram of wood dowel rotation welding.

2.5. Fourier-Transform Infrared Spectroscopy (FT-IR)

The molecular structure and functional groups of the welding interface were studied, and the chemical changesthatoccurred during welding were analyzed using a Varian 1000 (Varian, PaloAlto, CA, USA) infrared spectrometer [45–47]. The parameters for the analysis were as follows: wavenumber range of 400 to 4000 cm^{-1}; resolution set at 4 cm^{-1}; 32 scans per sample; ambient temperature maintained between 22 and 25 °C; and relative humidity of ≤60%.

2.6. X-ray Photoelectron Spectroscopy (XPS)

The chemical composition and element state of the welding interface and the chemical reaction that occurred in the welding process were investigated [45–47].The study utilized an X-ray photoelectron spectrometer (ThermoFischer, Waltham, MA, USA, model ESCALAB 250Xi) for analysis. The excitation source was a Ka line (Al: photon energy hv = 1486.6 eV). Full spectrum scans were conducted with a pass energy of 100 eV and a step size of 1 eV, while high-resolution scans had a pass energy of 50 eV and a step size of 0.05 eV. Samples were etched with argon ions for 10 s, followed by calibration of all binding energies using C1s = 284.80 eV as a reference. Data analysis was performed using Advantage 5.948 software.

2.7. X-ray Diffraction (XRD)

The crystal structure of the welding interface was analyzed, and the possible crystal phase change during welding was studied.The crystallinity of the Chinese fir base material at the welding site was analyzed using a TTR XRD from Rigaku Corporation, Tokyo, Japan. The parameters included a Cu target (λ = 0.154060 nm), a 2θ scanning range of 5 to 90°, step size of 0.02°, scanning rate of 5°/min, tube current of 120 mA, and tube voltage of 40 kV.

2.8. Scanning Electron Microscopy (SEM)

The morphology and microstructure of the welding interface were observed, and the bonding condition and defects of the welding interface were analyzed [45–47].The microscopic structure of the welding site and cross-section of the Chinese fir base material was observed using a Hitachi S-3400N Scanning Electron Microscope (Tokyo, Japan). An acceleration voltage of 12.5 kV was chosen, and the specimen surfaces were gold-sputtered for observation. Images at various magnifications (50×, 100×, 200×, 500×, 1000×, and 2000×) were captured and saved from the SEM.

3. Results and Discussion

3.1. Effect of Dowel-to-Guiding Hole Diameter Ratio on Welded Wood Performance

The impact of the dowel-to-guide hole diameter ratio on the performance of welded wood is exquisitely captured in Figure 2, which comprises three insightful sub-figures. Figure 2a demonstrates significant differences between the stress–strain curves of unwelded and welded wood, highlighting significant disparities. In unwelded wood, the stress–strain curve initially ascended to a peak, subsequently experiencing a precipitous decline, followed by fluctuations with a progressively diminishing amplitude. This behavior is attributed to the frictional forces between the wood fibers, reminiscent of those observed in connections made with round steel nails [4,11,20]. The rapid decline in the curve is attributed to the maximum static friction force prior to dowel extraction, where the primary tensile resistance originates from this maximal static friction (reaching the limit strength at the peak of static friction). As the dowel gradually extracts, the static friction transitions to kinetic friction. However, the contact area between the dowel and the substrate diminishes, leading to a reduction in kinetic friction that eventually transitions back to a smaller static friction. Throughout this process, the alternating static and kinetic frictions continuously erode the strength, resulting in the stress–strain curve's fluctuating yield with progressively diminishing peaks. Some studies attribute this oscillatory yielding phenomenon to stick-slip behavior [48,49], where the dowel extraction causes relative movement between the dowel and the substrate, necessitating overcoming the unevenness of the friction pair's rough surface, leading to fluctuations in frictional force, indicative of the repeated transitions between dynamic and static friction.

The welded Chinese fir's stress–strain curve lacks oscillatory yielding, suggesting its connection strength is not primarily friction-based. Figure 2b shows the dowels turning conical, indicating intense friction during welding, leading to increased temperature and lignin softening and melting. This process, involving partial entanglement, contributes to the wood's strength. However, the strength of these connections is initiated by friction

but not exclusively derived from it, implying a more complex interplay of factors in the strength of welded wood.

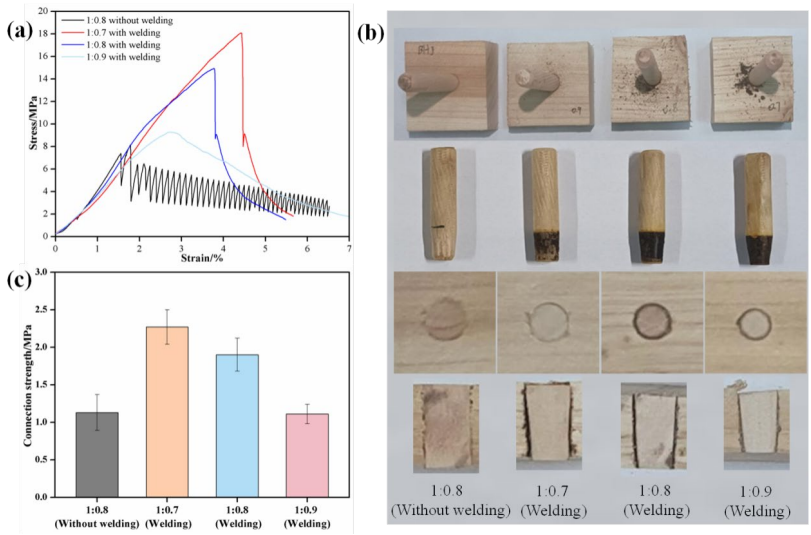

Figure 2. Diameter ratio of wooden dowel to guiding bore. Note: (**a**) stress–strain curve, (**b**) cross-section image, and (**c**) connection strength.

Figure 2c reveals that the highest tensile resistance is achieved with a diameter ratio of 1:0.7, reaching 2.27 MPa. With a ratio of 1:0.8, the tensile resistance decreased to 1.90 MPa, further reducing to 1.11 MPa with a ratio of 1:0.9, slightly higher than the connection strength of unwelded wood (diameter ratio 1:0.8) at 1.13 MPa. This indicates that a greater connection strength can be obtained through pure dowel welding than through unwelded connections. It was caused by the following: (1) Friction heat generation and distribution: When the diameter is relatively small, the contact between the dowel and the guide hole is closer, resulting in the concentrated generation of friction heat and a more uniform heat distribution. This increases the degree of softening of the lignin and promotes the fusion and mechanical interlocking of the wood fibers, thus improving the firmness of the connection. (2) Fiber melting and mechanical interlocking: When the diameter is small, friction heat can make the fiber on the surface of the dowel reach the melting temperature faster, promoting the rearrangement and mosaic of the fiber. A larger diameter ratio may result in insufficient heat to completely soften the lignin, thus affecting the quality of the weld. (3) Heat transfer: When the dowel diameter is larger, the heat generated by welding is lower, and the heat conduction is blocked, resulting in a lower temperature in the welding zone.

To sum up, the diameter ratio of the wood dowel to the guide hole plays a key role in the welding process, and too large or too small a diameter ratio is not conducive to the generation, distribution, transfer of heat, and fusion between wood fibers. Therefore, in practical applications, it is necessary to optimize the diameter ratio to ensure the best welding effect and the highest connection strength.

3.2. Effect of Welding Standing Time on the Performance of Welded Wood

The study depicted in Figure 3 investigates the influence of dwell time during rotational dowel welding at a predetermined depth on wood performance. Figure 3a reveals that the tensile pull-out strength is highest with no dwell time (1.88 MPa), and decreases as dwell time extends, dropping to 1.28 MPa at 1 s and further to 0.85 MPa at 2 s. This decline in strength withanincreased dwell time suggests that excessive heating in the welding area may cause wood damage, reducing tensile strength. The further decrease at 2 s could be due to more severe thermal damage or degradation, potentially compromising the wood's fibrous structure and reducing the effective mechanical interlocking between the dowel and the hole wall.

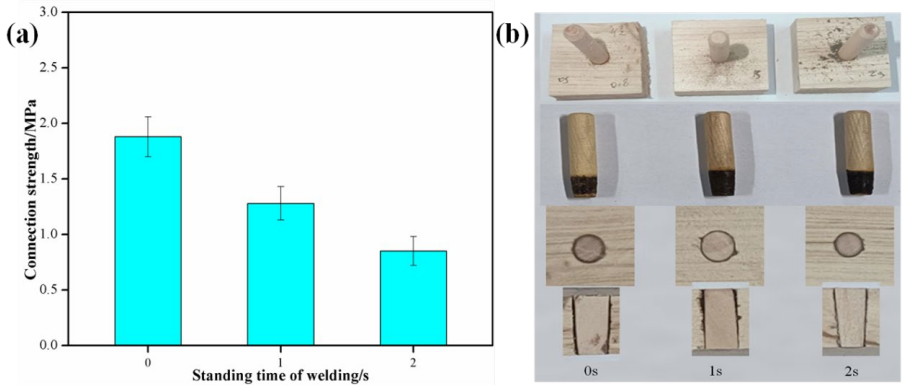

Figure 3. Effect of welding standing time on the performance of welded wood. Note: (**a**) Connection strength, (**b**) status of welded wood.

Figure 3b demonstrates a clean substrate surface at zero seconds dwell time, with an increase in charring observed at two seconds. Longer dwell times result in more severe dowel burning and a tendency for the dowel to become more conical, leading to unevenness and increased gaps at the interface. This suggests a competitive dynamic in the welding process; effective melting and mechanical interlocking between the dowel and the hole wall enhance connection strength, while the heat generated by welding can cause wood damage, reducing the strength of the connection. Brief welding may suffice for optimal melting and interlocking without causing excessive thermal damage, whereas longer dwell times can increase the potential for thermal decomposition and carbonization of the dowel, weakening the connection.

3.3. Effect of Welding Depth on the Performance of Welded Wood

The impact of the rotational welding depth of dowels on the performance of welded wood is shown in Figure 4. As illustrated in Figure 4a, the connection strength increases from 1.44 MPa at 15 mm to 1.83 MPa at 20mm but plateaus at 1.82 MPa at a 25 mm depth. This suggests that while increased depth theoretically enlarges the contact area, enhancing mechanical interlocking, adepth increment beyond 20 mm does not significantly improve strength. This could be due to consistent dowel friction wear and uneven heat distribution at greater depths, underscoring the importance of optimal depth for quality welding.

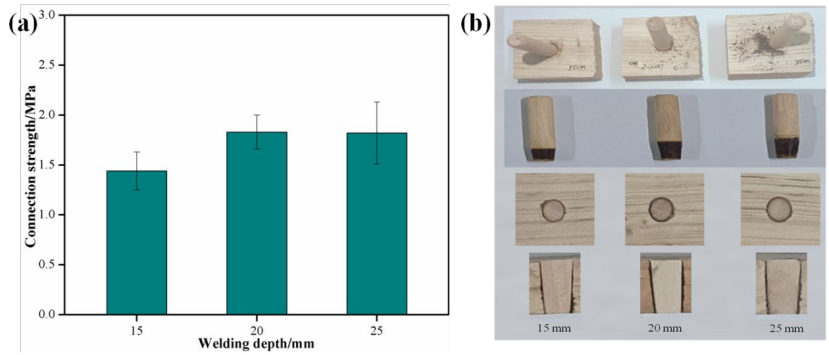

Figure 4. Effect of welding depth on the performance of welded wood. Note: (**a**) Connection strength, (**b**) status of welded wood.

Figure 4b reveals minimal dowel wear and tighter interlocking between the dowel and hole wall at a 20 mm depth. This depth appears to balance material wear and heat distribution effectively, fostering a conducive environment for thermal decomposition and fusion without excessive heat loss or uneven transfer. However, a depth of 25 mm may surpass the ideal welding depth, leading to inconsistent heat distribution and potentially affecting tensile strength due to overheating or insufficient heating. The observed

increase inthestandard deviation at greater depths hints at the variability in connection strength, possibly linked to the complexity of manual operations or material inconsistencies. Therefore, the selection of an appropriate welding depth is essential for achieving optimal welding performance.

3.4. Effect of Welding Base Surface on Welded Wood Performance

Figure 5 presents the performance test results of welded wood on cross-cut, radial-cut, and tangential-cut surfaces. As Figure 5a,c shows, the stress–strain curve trends during dowel extraction are consistent across these surfaces. The radial-cut surface exhibited the highest tensile pull-out strength (1.85 MPa), followed by the tangential-cut (1.1 MPa), and the lowest in the cross-cut surface (0.97 MPa).

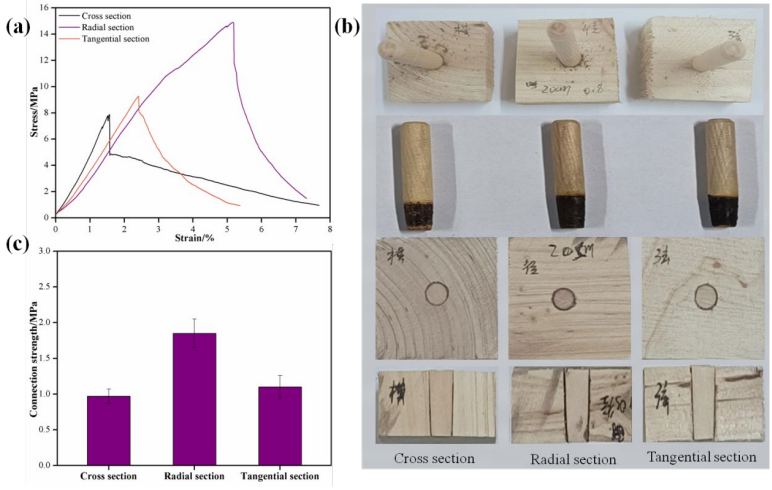

Figure 5. Effect of welding base surface on the performance of welded wood. Note: (**a**) stress–strain curve, (**b**) status of welded wood, and (**c**) Connection strength.

The anisotropic nature of wood, characterized by variations in density, porosity, and fiber alignment across different base surfaces, significantly impacts heat conduction and distribution during the welding process. This, in turn, influences the quality of the weld. On cross-cut surfaces, where fibers predominantly run parallel to the longitudinal axis and are interconnected by hydrogen bonds, the dowel aligns with these fibers. This orientation means that frictional forces are largely dependent on fiber compression, leading toacomparatively lower tensile strength. Elements such as growth rings and rays can induce uneven heating and thermal stress concentration in the welding area, potentially causing cracks or insufficient welding. Moreover, the compression force exerted during the cooling phase post-welding is perpendicular to the fiber direction on cross-cut surfaces, which may preventthetight interlocking of fibers and consequently decrease tensile strength.

In radial-cut and tangential-cut surfaces, the dowel imparts a shearing action on wood fibers. This shearing effect means that friction is largely influenced by the wood fibers' resistance to shear, leading to a notably higher tensile strength compared to cross-cut surfaces. The radial-cut surface, with its fiber alignment parallel to the welding pressure, facilitates tighter fiber entwining and interlocking, which accounts for its superior tensile strength over the tangential-cut surface. Variations in earlywood and latewood, arrangement patterns, lignin content, and microfibril orientation in radial and tangential cuts also contribute to differences in tensile strength [4,11,28–31].

The different welding base surfaces' performance variation underscores the importance of the substrate fibers' direction on heat generation and transfer, as well as the interlocking of melted products. In practical applications, selecting the correct base surface is vital for ensuring optimal welding quality and the strength of the connection. This decision is pivotal, as it directly impacts the effectiveness of the welding process and the durability of the welded joint.

3.5. Effect of Welding Angle on the Performance of Welded Wood

The relationship between the rotational welding angles of dowels and the performance of welded wood is depicted in Figure 6. It was observed that at 90°, the tensile pull-out strength peaked at 1.89 MPa. However, this strength decreased to 1.12 MPa at 60° and dropped further to the lowest point of 0.9 MPa at 45°. Interestingly, an increase in strength to 1.67 MPa was noted at 30°. This trend suggests that while the contact area between the dowel and guide hole grows with a decreasing welding angle, the tensile strength demonstrates a non-linear relationship, initially decreasing and then increasing.

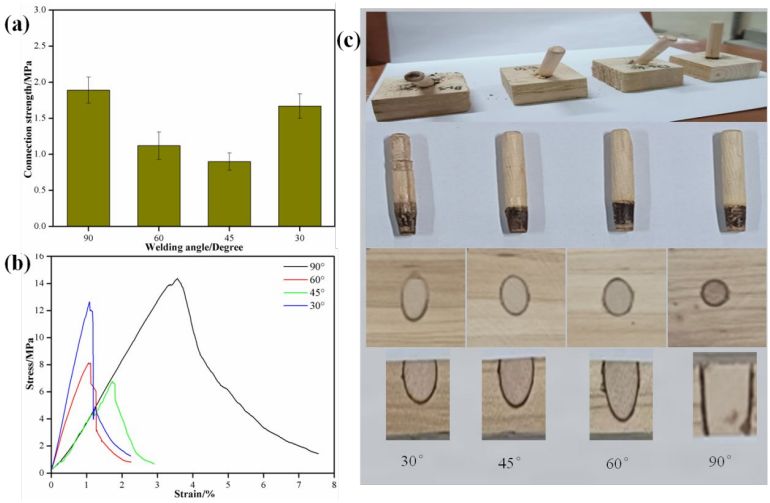

Figure 6. The effect of welding angle on the performance of welded wood. Note: (**a**) Connection strength, (**b**) stress–strain curve, and (**c**) status of welded wood.

In Figure 6c, the welding at 90° shows the smallest contact area and relative depth, concentrating the heat and maximizing strength. At 60° and 45°, the increased contact area and depth facilitate efficient heat distribution and wood thermal degradation, affecting tensile strength. A significant strength increase from 45° to 30°, by 67%, suggests enhanced fiber entanglement and mechanical interlocking due to the largest contact area and depth. The welding at 90° involves the radial surface, whereas, at 60°, 45°, and 30°, it is a mix of cross-cut and tangential-cut surfaces, resulting inalower strength than radial-cut welding. Stability in welding performance at 90° is also evident from Figure 6b.

The welding angle significantly affects heat distribution in the process, influencing the thermal decomposition and formation of chemical bonds between the dowel and substrate. It also alters the internal stress distribution within the wood, impacting the fiber's interlocking mechanism and overall strength. Consequently, the choice of welding angle is vital for the strength of the welded wood joints. Ensuring the selection of an appropriate welding angle is crucial to maintaining the quality of welding and the strength of the joints in practical applications.

3.6. Effect of Different Dowels on the Performance of Welded Wood

The welding performance of Schima superba, Beech, and Eucalyptus dowels shows distinct results, as illustrated in Figure 7. Eucalyptus dowels demonstrated the highest tensile pull-out strength at 2.13 MPa, surpassing Schima superba at 1.85 MPa and Beech at 1.38 MPa, indicating the most robust joint strength in Eucalyptus. This superior performance is attributed to the greater density and hardness of Eucalyptus, which contributes to enhanced stability and joint strength during welding. Further, Eucalyptus dowels maintain their shape better during the welding process, with minimal charring or deformation, and exhibit a smoother surface. The connection interface showed a tighter fit, and cross-sectional views displayed increased melting and interlocking of fibers, enhancing the mechanical interlocking.

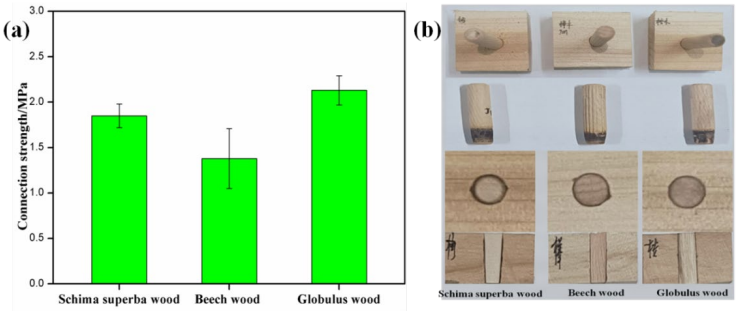

Figure 7. The influence of different tenon-and-mortise joints on the performance of welded wood. Note: (**a**) Connection strength, (**b**) status of welded wood.

Beech and Schima superba, despite their similar densities, exhibited notable differences in tensile strength. Beech's tensile strength was approximately 25% lower than that of Schima superba, with a more significant standard deviation. This discrepancy is primarily due to the coarser surface texture of Beech, which leads to increased wear during the rotational welding process, adversely affecting the connection's strength and stability. Furthermore, the variations in thermal decomposition temperatures and the nature of the decomposition products of different wood types can impact the structural integrity and strength of the welded interface. These findings underscore the importance of selecting appropriate dowel materials and welding parameters to ensure optimal performance in wood welding connections.

3.7. XPS Analysis

XPS analysis is a surface analysis technique that identifies the surface chemical composition and the chemical state of elements by measuring the binding energy of elements on the surface of a material. It is essential to understand how materials respond to external processing, such as welding, at both chemical and physical levels. The use of XPS in this study can reveal chemical changes on wood surfaces during welding, especially surface modifications related to wood welding techniques, such as oxidation–reduction reactions, the formation or breaking of chemical bonds, and so on.

Figure 8 displays the X-ray photoelectron spectroscopy (XPS) full spectrum for both unwelded and welded wood. The unwelded wood's atomic percentages for carbon, oxygen, and nitrogen are consistent with its primary components of cellulose, hemicellulose, and lignin. Welded wood shows a marginal variation in these percentages, reflecting a slight decrease in carbon and increases in oxygen and nitrogen. These changes imply that welding's intense heat and pressure have modified the surface chemistry of the wood, potentially altering its chemical structure and forming new chemical bonds.

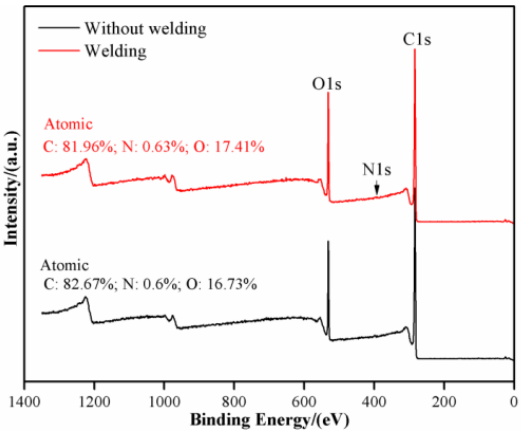

Figure 8. XPS full spectrum.

Figure 9 presents high-resolution spectra for C1s, O1s, and N1s of both unwelded and welded wood, revealing significant chemical state alterations on the wood surface post-welding. From the C1s spectral, it can be seen that the spectral lines of unwelded wood and welded wood wereslightly different in terms ofthecarbonization environment. This suggests that welding may lead to changes in the chemical environment of the surface carbon compounds, such as the increase or decrease in C-O and C=O bonds [45,46]. This change may be due to the thermal decomposition of wood components, such as lignin and cellulose, caused by high temperatures during the welding process. The O1s spectral shows that welded wood hadmore oxidation forms than unwelded wood, such as C=O and O-C=O [47,48]. This indicates that the welding process may increase the degree of oxidation of the wood surface, which may be related to the contact of oxygen and the high-temperature environment during the welding process. The N1s spectrum of unwelded wood showedapeak of C-NH_2 functional groups, and the welded wood showeda new O=N-O peak, indicating that the welded wood shows a more complex nitrogen chemical environment than the unwelded wood, possibly due to the materials used in the welding process or the nitrogen sources in the environment.

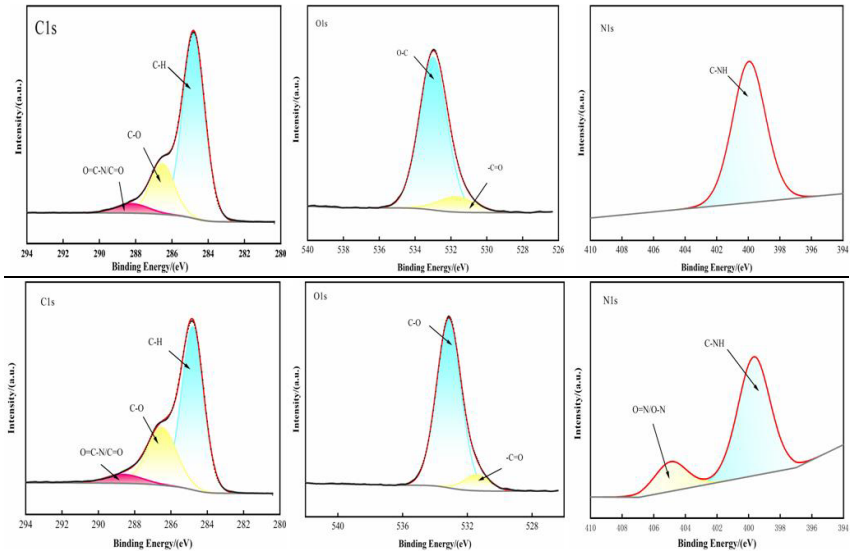

Figure 9. XPS peaks fitting diagram.

In essence, the welding process, characterized by elevated temperatures and pressures, potentially alters the chemical composition of the wood's surface. This alteration encompasses modifications in chemical structures and the emergence of new chemical bonds, reflecting the profound impact of the welding conditions on the wood's chemistry.

3.8. XRD Analysis

XRD analysis is mainly used to evaluate the crystal structure of materials, especially in exploring the effect of the welding process on the crystal structure of wood. In this study, XRD analysis can reveal the changes in the crystal structure of Chinese fir before and after welding, which helping to understand how the physical and chemical changes during welding affect the structure and final properties of the material.

Figure 10 shows the XRD curves of unwelded and welded wood. The XRD showed a significant difference in the crystal structure of the unwelded and the welded Chinese fir. The unwelded wood showed a lower crystallinity (13.6%), while the crystallinity of the welded wood increased significantly to 69.4%. This suggests that the high temperatures generated during welding may prompt some of the amorphous regions in the fir to rearrange into a more ordered crystal structure. The peaks of the welded wood at 22.2° and 34.5° are obvious, and these peaks correspond to the enhancement of the reflection of the specific crystal surface, indicating that the formation or growth of the crystal surface

may be promoted during the welding process. The ordering of the crystal structure after welding usually means that the mechanical properties of the material may be improved, such as increased hardness and increased compressive strength. The increased crystallinity may also have a positive impact on the thermal stability and durability of the material. The change incrystal structure is directly related to the quality and durability of the welded area. The more ordered crystal structure helps to improve the load transfer capacity and environmental resistance of wood joints.

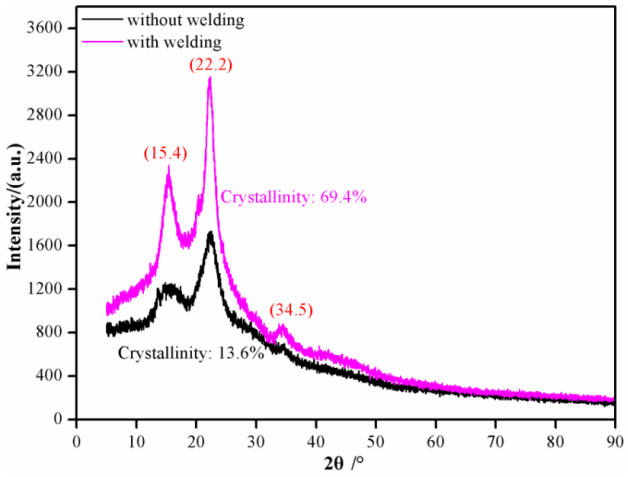

Figure 10. XRD curves of wood surface.

3.9. FTIR Analysis

Figure 11 illustrates the infrared spectral analysis of Chinese fir wood, both unwelded and welded. The spectral profile, dominated by cellulose, lignin, and hemicellulose, reveals distinct peaks: O—H stretching vibrations at 3417.4 cm^{-1}, C—H stretching in various groups at 2906.7 cm^{-1}, and the characteristic C=O stretching of hemicellulose and lignin at 1732.0 and 1650.7 cm^{-1}, respectively. Additionally, the spectrum indicated lignin's phenylpropane structure through C—C vibrations between 1426.0 and 1511.5 cm^{-1} and C—O bending at 1270.3 cm^{-1}. Cellulose's signature wasevident in C—O—C and C—OH vibrations at 1157.9 and 1110.5 cm^{-1}, complemented by C—O stretching peaks at 1059.8 and 1032.5 cm^{-1}. Further, the C—H bending of cellulose, hemicellulose, and mannose were observed at 896.7 and 811.0 cm^{-1}, with lignin's phenylpropane structure C—H bending in the 526.3 to 668.9 cm^{-1} range.

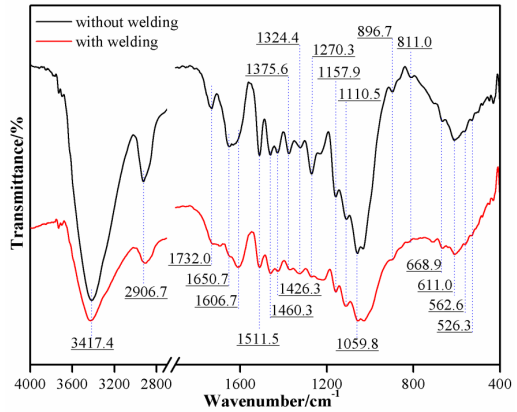

Figure 11. FT-IR curves of welded wood.

In the welded Chinese fir interface, the diminished intensities at 3417.4 and 2906.7 cm^{-1} indicate lignin's thermal decomposition during welding [50–53]. This process results in dehydration among hydroxyl groups in cellulose's amorphous sections, as evidenced

by reduced hydroxyl concentrations near 3417.4 cm^{-1}. Hemicellulose demonstrated notable thermal instability, reflected bythe significant decrease in peak intensities at 1732.0, 1059.8, 896.7, and 811.0 cm^{-1}, with its content markedly diminished. Lignin, however, exhibited comparative stability throughout the process, suggested by minimal peak variations.The spectral analysis revealed minimal fluctuations within the 1426.0~1511.5 cm^{-1} and 526.3~668.9 cm^{-1} ranges, indicating lignin's relative stability amidst the welding process. These findings suggest the absence of pronounced degradation in lignin's structure, underscoring its resilience to the thermal conditions encountered during welding. Interestingly, the peaks at 1157.9 and 1110.5 cm^{-1} were pronouncedly enhanced, implying that cellulose remains structurally intact, possibly even undergoing increased intermolecular entanglement and crosslinking under welding conditions, thereby augmenting its crystallinity. Thus, the welding process primarily leads to moisture evaporation and hemicellulose thermal decomposition, potentially inducing a reconfiguration of the molecular structure in lignin and cellulose, as manifested in the altered characteristic absorption peaks in the infrared spectrum.

3.10. SEM Analysis

Figure 12 provides SEM imagery of both unwelded and welded wood at the welding junction. The unwelded wood exhibited a smooth surface at a magnification of ×4000, while at ×1000, additional surface details became evident, maintaining uniformity. At a broader view of ×150 magnification, the overall surface condition wasshown, displaying a clear wood texture. This contrast in surface detail at varying magnifications offers a comprehensive view of the wood's structural changes at the microscopic level, particularly evident in the welding point's transformations.

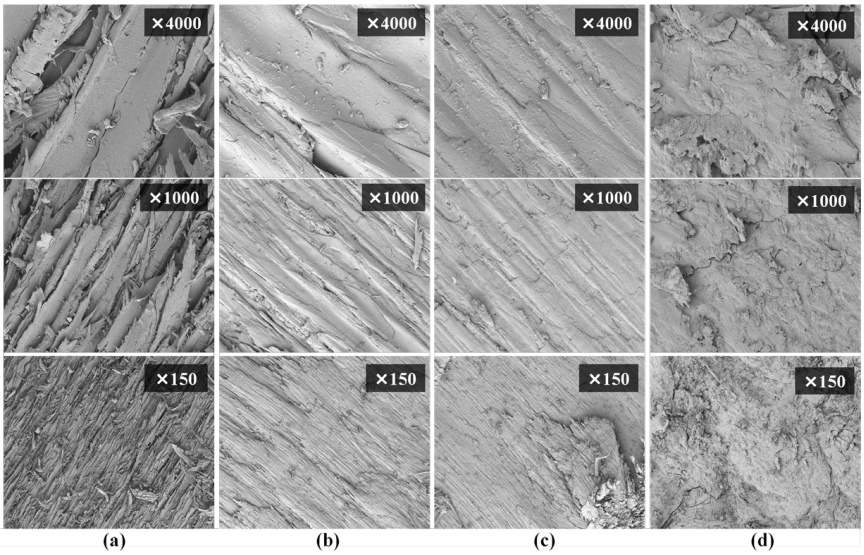

Figure 12. SEM image of welding sites. Note: (**a**) control; (**b**) standing time of 0s; (**c**) standing time of 1s; (**d**) standing time of 2s.

In the welded wood at 0 s of dwell time, the SEM images at a magnification of ×4000 revealed the onset of microstructural changes, characterized by small melting areas. The finer melting textures observed at ×1000 magnification indicate the commencement of welding, with a relatively confined heat-affected zone. At a lower magnification of ×150, the imagery showed minimal macroscopic alterations, underscoring the limited impact of short-duration welding on the wood's overall structure. This suggests that brief welding durations initiate subtle yet distinct changes at the micro level.

At 1 s of dwell time, the SEM images at ×4000 magnification revealed more pronounced melting and solidification, indicating intensified welding effects. At ×1000, distinct heat-affected and molten textures wereevident, marking the progression of the

welding process. The macroscopic distinction between welded and unwelded areas became apparent at ×150 magnification. At 2 s, the ×4000 magnification displayed extensive solidified textures, signifying substantial thermal effects and material flow. The ×1000 magnification showed clear molten pools and solidification textures, while at ×150, the most pronounced macroscopic welding effects werevisible with distinct boundaries between welded and unwelded areas.

In conclusion, the initial phase of dowel welding in wood exhibits minor microstructural changes, primarily due to the formation of small melt pools that rapidly cool. Prolonged welding times increased heat generation, and which resulted in larger melt pools and more pronounced heat-affected zones. This escalation in heat and melting significantly alters the microstructure, with potential implications for the wood's crystalline structure, illustrating the crucial balance between welding duration and microstructural integrity.

Figure 13's SEM images distinctly showcase the interface between unwelded and welded wood. In the unwelded wood, the edges where the dowel and substrate meet weresharply defined, without any noticeable blending of materials or changes in morphology. The ×50 magnification highlighted a pronounced gap between the dowel and substrate, and this gap wasfurther detailed in the ×100 magnification, showcasing the stark difference in the interaction at the interface in unwelded wood.

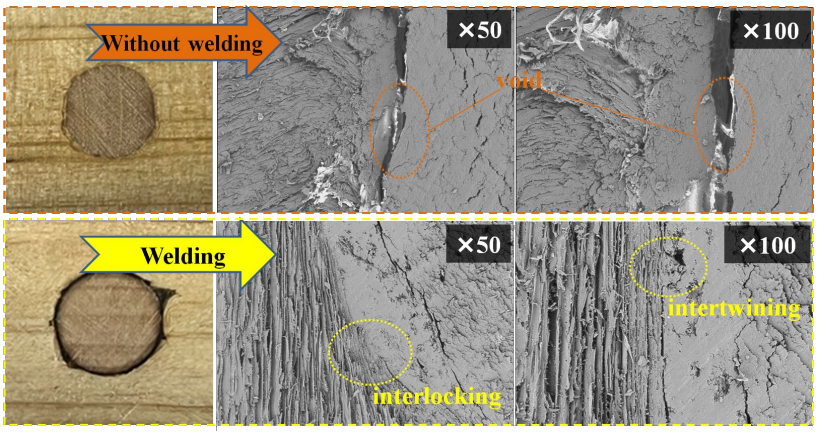

Figure 13. SEM curves of welding surface.

In the welded wood, SEM images depicted a less distinct interface, signaling a level of material fusion. This was evident in both ×50 and ×100 magnifications, where the wood fibers wereseen to be tightly connected and entwined, highlighting a significant microscopic-scale dissolution and embedding. The visual data thus underscores the substantial change in wood structure upon welding, reflecting the intricacies of the welding process at a microscopic level.

The high temperatures generated during welding lead to the melting of wood fiber surfaces, enhancing the interface's compactness as fibers intertwine and embed into each other. This process creates a complex physical structure at the welding interface, where mechanical interlocking between fibers increases bonding strength. Additionally, the heat softens the wood fibers, causing partial decomposition and releasing components like lignin, cellulose, and hemicellulose. These components may undergo chemical changes under high temperatures, forming new chemical bonds that strengthen the adhesion between the dowel and substrate. The pressure applied during welding also promotes tighter fiber contact and mechanical interlocking. As the wood cools post-welding, the softened material solidifies, locking in the physical combination and forming a stable welded joint. Overall, the welding process's heat and pressure not only facilitate physical interlocking among wood fibers but may also enhance interface bonding strength through chemical changes.

4. Conclusions

This study, utilizing Guizhou's native Chinese fir, focused on how factors such as dowel-to-guide hole diameter ratio, welding time, depth, base surface, angle, and dowel type influence the performance of welded Chinese fir. It analyzed the physical and chemical changes at the welding interface. The key findings include the following:

(1) Significant thermolysis, especially in hemicellulose, occurred post-rotational welding. The generated heat facilitated good melting and mechanical interlocking between the dowel and hole wall, coupled with frictional losses of the dowel and substrate;
(2) The aforementioned factors variably affect the welding wood's connection strength and stability through their influence on heat generation, distribution, transfer, and frictional losses. Nevertheless, the mechanism of friction temperature influence is very complicated; more in-depth and systematic studies arenecessary in the following work;
(3) Changes in the chemical composition at the welding interface were observed, with more orderly crystalline binding and tight, gapless joints enhancing the connection strength;
(4) This study underscores the industrial production potential of welded Chinese fir and lays the foundation for enhancing welding techniques and performance.

Author Contributions: Validation, investigation, resources, X.X., D.Y., J.P., X.Z. (Xin Zhao), W.G., S.Y., G.Y. and F.G.; conceptualization, methodology, writing—original draft preparation, X.Z. (Xiao Zhong), D.L. and Q.L.; formal analysis, writing—review and editing, supervision, Z.W. and J.L. All authors have read and agreed to the published version of the manuscript.

Funding: This work was supported by the Science–Technology Support Foundation of the Guizhou Province of China ([2019]2308 and [2020]1Y128), the Forestry Science and Technology Research Project of the Guizhou Forestry Bureau, China ([2020]C14), the Qiandongnan Basic Research Program Project ([2021]15), the Outstanding Youth Science and Technology Talent Project of Guizhou Province, China (YQK[2023]003), the Talents from Guizhou Science and Technology Cooperation Platform ([2019]01-3), the Kaili University 'Practical Engineering' Special Project (2020gkzs01), Youth Science and Technology Talent Project of Guizhou Province [2020]181, the Agriculture Joint Research Program of Yunnan Province (2017FG001(-079)), and the International Joint Research Center for Biomass Materials Open Fund (2023-GH03 and 2023-GH05).

Data Availability Statement: All the data are provided in the manuscript.

Conflicts of Interest: The authors declare no conflicts of interest.

References

1. De Araujo, V.; Aguiar, F.; Jardim, P.; Mascarenhas, F.; Marini, L.; Aquino, V.; Santos, H.; Panzera, T.; Lahr, F.; Christoforo, A. Is Cross-Laminated Timber (CLT) a Wood Panel, a Building, or a Construction System? A Systematic Review on Its Functions, Characteristics, Performances, and Applications. *Forests* **2023**, *14*, 264. [CrossRef]
2. Liu, M.; Murano, A.; Goh, C.S.; Kayo, C. Evaluation of the Environmental Burden of Cross-Laminated Timber Manufacturing in Japan Using the Input–Output Analysis. *Forests* **2023**, *14*, 2263. [CrossRef]
3. Wang, J.; Wei, P.; Gao, Z.; Dai, C. The evaluation of panel bond quality and durability of hem-fir cross-laminated timber (CLT). *Eur. J. Wood Prod.* **2018**, *76*, 833–841. [CrossRef]
4. Li, D.; Yu, L.; Li, L.; Liang, J.; Wu, Z.; Yang, G.; Yin, S.; Gong, F. Comparison of nail-holding performance of Pinus massoniana and Cunninghamia lanceolata dimension lumber based on round steel nails. *Bioresources* **2024**, *19*, 670–682. [CrossRef]
5. Sonne, C.; Xia, C.; Lam, S. Is engineered wood China's way to carbon neutrality? *J. Bioresour. Bioprod.* **2022**, *7*, 83–84. [CrossRef]
6. Huang, H.; Gao, Y.; Chang, W.S. Human-induced vibration of cross-laminated timber (CLT) floor under different boundary conditions. *Eng. Struct.* **2020**, *204*, 110016. [CrossRef]
7. Li, H.; Wang, B.; Wei, P.; Wang, L. Cross-laminated timber (CLT) in China: A state-of-the-art. *J. Bioresour. Bioprod.* **2019**, *4*, 22–31. [CrossRef]
8. Liu, M. *Study on Surface Strengthening Technology of Fast-Growing Fir and Its Adhering Capacity of Coating*; Central South University of Forestry and Technology: Changsha, China, 2017.
9. Jia, D.; Fu, Y.; Su, Z.; Dong, H.; Tang, L.; Shi, Y. Optimized Production Technology for Fine Surface Oriented Strand Board from Chinese Fir. *China Wood-Based Panels* **2023**, *30*, 17–20.

10. Li, N.; Zhang, S.; Li, X.; Yuan, Q.; Wang, C.; Cheng, F. Study on the preparation of Chinese fir three-layer composite flooring substrate based on glue wire connection. *Papermak. Equip. Mater.* **2021**, *50*, 50–52.
11. Li, D.; Zhang, B.; Tu, Y.; Xiao, G.; Tian, M.; Xu, X.; Zhong, X.; Zhang, Q.; Wu, Z.; Liang, J. Nail holding Performance of self-tapping screws on Masson pine and Chinese fir dimension lumbers. *J. Renew. Mater.* **2023**, *11*, 3725–3738. [CrossRef]
12. Wang, F.; Liu, J.; Lyu, W. Effect of boron compounds on properties of Chinese fir wood treated with PMUF resin. *J. Bioresour. Bioprod.* **2019**, *4*, 60–66. [CrossRef]
13. Abdoli, F.; Rashidi, M.; Rostampour-Haftkhani, A.; Layeghi, M.; Ebrahimi, G. Withdrawal performance of nails and screws in cross-laminated timber (CLT) made of poplar (*Populus alba*) and fir (*Abies alba*). *Polymers* **2022**, *14*, 3129. [CrossRef] [PubMed]
14. Sun, H.; Gong, Y.; Yan, Y.; Li, S.; Fu, C.; Chang, X.; Chen, T. Effect of delignification on cell wall structure of fast-growing poplar and Chinese fir. *J. For. Eng.* **2023**, *8*, 46–54.
15. Li, X.; Lin, J.; An, X.; Zhou, B.; Huang, H.; Que, Z. Effect of hot-pressing parameters on recovery rate and mechanical properties of Chinese fir compressed wood. *J. For. Eng.* **2023**, *8*, 37–45.
16. Wang, Y.; Lee, S.H. A theoretical model developed for predicting nail withdrawal load from wood by mechanics. *Eur. J. Wood Wood Prod.* **2018**, *76*, 973–978. [CrossRef]
17. Barcík, Š.; Gašparík, M.; Horejš, P. Influence of thermal modification on nail withdrawal strength of spruce wood. *Bioresources* **2014**, *9*, 5963–5975. [CrossRef]
18. Chen, G.; Wang, C.; Wu, J.; Zhang, E.; Wu, D. Mechanical performance of nailed connections between laminated bamboo lumber and oriented strand board. *J. For. Eng.* **2023**, *8*, 75–81.
19. Li, P.; Yang, C.; Jiang, Z.; Jin, Y.; Wu, W. Lignocellulose pretreatment by deep eutectic solvents and related technologies: A review. *J. Bioresour. Bioprod.* **2023**, *8*, 33–44. [CrossRef]
20. Zhang, Z.; Tang, S.; Cui, Z. Experimental study on the pull-through performance of self-tapping screws in laminated bamboo. *J. For. Eng.* **2023**, *8*, 40–45.
21. Yuri, I.; Golovin, A.; Gusev, D.; Golovin, S.; Matveev, A.; Tyrin, A.; Samodurov, V.; Korenkov, I.; Vasyukova, M. Multiscale wood micromechanics and size effects study via nanoindentation. *J. Bioresour. Bioprod.* **2023**, *8*, 246–264.
22. Pizzi, A.; Mansouri, H.R.; Leban, J.M.; Delmotte, L.; Pichelin, F. Enhancing the exterior performance of wood joined by linear and rotational welding. *J. Adhes. Sci. Technol.* **2011**, *25*, 2717–2730. [CrossRef]
23. Yin, W.; Lu, H.; Zheng, Y.; Tian, Y. Tribological properties of the rotary friction welding of wood. *Tribol. Int.* **2022**, *167*, 107396. [CrossRef]
24. Zhang, J.; Gao, Y.; Zhang, J.; Zhu, X. Influence of pretreated wood dowel with $CuCl_2$ on temperature distribution of wood dowel rotation welding. *J. Wood Sci.* **2018**, *64*, 209–219. [CrossRef]
25. Zhu, X.; Gao, Y.; Yi, S.; Ni, C.; Zhang, J.; Luo, X. Mechanics and pyrolysis analyses of rotation welding with pretreated wood dowels. *J. Wood Sci.* **2017**, *63*, 216–224. [CrossRef]
26. Vaziri, M.; Sandberg, D. Welding of thermally modified wood and thermal modification of the welded wood: Effects on the shear strength under climatic conditions. *Bioresources* **2021**, *16*, 3224–3234. [CrossRef]
27. Suthoff, B.; Schaaf, A.; Hentschel, H. Method for Joining Wood. Patent DE 19620273, 27 November 1997.
28. Gfeller, B.; Properzi, M.; Zanetti, M.; Pizzi, A.; Pichelin, F.; Lehmann, M.; Delmotte, L. Wood bonding by mechanically-induced in situ welding of polymeric structural wood constituents. *J. Appl. Polym. Sci.* **2004**, *92*, 243–251. [CrossRef]
29. Delmotte, L.; Ganne-Chedeville, C.; Leban, J.M.; Pizzi, A.; Pichelin, F. CP-MAS ^{13}C-NMR and FT-IR investigation of the degradation reactions of polymer constituents in wood welding. *Polym. Degrad. Stab.* **2007**, *93*, 406–412. [CrossRef]
30. Pizzi, A.; Leban, J.M.; Kanazawa, F.; Properzi, M.; Pichelin, F. Wood dowel bonding by high-speed rotation welding. *J. Adhes. Sci. Technol.* **2004**, *18*, 1263–1278. [CrossRef]
31. Kanazawa, F.; Pizzi, A.; Properzi, M.; Delmotte, L.; Pichelin, F. Parameters influencing wood-dowel welding by high-speed rotation. *J. Adhes. Sci. Technol.* **2005**, *19*, 1025–1038. [CrossRef]
32. Jia, H.; Gao, Y.; Meng, X.; Yang, H.; Zhang, Y.; Xu, F. Shear tests and theoretical analysis of wood-dowel rotation welding joints. *J. For. Eng.* **2022**, *7*, 38–44.
33. Belleville, B.; Stevanovic, T.; Pizzi, A.; Cloutier, A.; Blanchet, P. Determination of optimal wood-dowel welding parameters for two North American hardwood species. *J. Adhes. Sci. Technol.* **2013**, *27*, 566–576. [CrossRef]
34. Cornuault, P.H.; Carpentier, L. Tribological mechanisms involved in friction wood welding. *Tribol. Int.* **2020**, *141*, 105963. [CrossRef]
35. Župčić, I.; Vlaović, Z.; Domljan, D.; Grbac, I. Influence of Various Wood Species and Cross-Sections on Strength of a Dowel Welding Joint. *Drv. Ind.* **2014**, *65*, 121–127. [CrossRef]
36. Pizzi, A.; Leban, J.M.; Zanetti, M. Surface properties and penetration of wood dowel welding. *J. Adhes. Sci. Technol.* **2004**, *18*, 673–686.
37. Belleville, B.; Stevanovic, T.; Cloutier, A. Effects of mechanical properties and surface roughness on the strength of wood dowel welded joints. *Holzforschung* **2016**, *70*, 159–166.
38. Omrani, P.; Pizzi, A.; Delmotte, L. Influence of grain direction and preheating on the tensile shear strength of linear friction welding of wood. *Eur. J. Wood Wood Prod.* **2009**, *67*, 211–213.
39. Pizzi, A.; Despres, A.; Mansouri, H.R.; Leban, J.M.; Rigolet, S. Wood joints by through-dowel rotation welding: Microstructure, ¹³C-NMR and water resistance. *J. Adhes. Sci. Technol.* **2006**, *20*, 427–436.

40. Pizzi, A.; Zhou, X.; Navarrete, P.; Segovia, C.; Mansouri, H.R.; PlacentiaPena, M.I.; Pichelin, F. Enhancing water resistance of welded dowel wood joints by acetylated lignin. *J. Adhes. Sci. Technology* **2013**, *27*, 252–262. [CrossRef]
41. Omrani, P.; Pizzi, A.; Mansouri, H.R.; Leban, J.-M.; Delmotte, L. Physico-chemical Causes of the Extent of Water Resistance of Linearly Welded Wood Joints. *J. Adhes. Sci. Technol.* **2009**, *23*, 827–837. [CrossRef]
42. Wang, J.; Jin, H. Research Progress of Wood Friction Welding Technology. *J. Northwest For. Univ.* **2019**, *34*, 191–196.
43. Amirou, S.; Pizzi, A.; Delmotte, L. Citric acid as water proofing additive in butt joints linear wood welding. *Eur. J. Wood Wood Prod.* **2017**, *75*, 651–654. [CrossRef]
44. Amirou, S.; Pizzi, A.; Belleville, B.; Delmotte, L. Water resistance of natural joint of spruce produced by linear friction welding without any treatment. *Int. Wood Prod. J.* **2017**, *8*, 201–207. [CrossRef]
45. Yang, H. *Research of Bamboo Dowel Rotary Welding Process and Joints Mechanical Properties*; Beijing Forestry University: Beijing, China, 2022.
46. Li, S.; Zhang, H.; Cheng, L.; Ju, Z.; Lu, X. Bonding Properties of Bamboo Dowel (Nail) Welded to Wood with High Speed Rotation. *J. Northwest For. Univ.* **2021**, *36*, 225–232+248.
47. Zhu, X.; Xue, Y.; Zhang, S.; Shen, J.; Gao, Y. Influence Mechanisms of Welding Time and $CuCl_2$ Treatment on the Weldability of Dowels. *J. Northwest For. Univ.* **2019**, *34*, 231–239.
48. Sun, Y.; Royer, M.; Diouf, P.N.; Stevanovic, T. Chemical changes induced by high-speed rotation welding of wood application to two Canadian hardwood species. *J. Adhes. Sci. Technol.* **2010**, *24*, 1383–1400. [CrossRef]
49. Delmotte, L.; Mansouri, H.R.; Omrani, P.; Pizzi, A. Influence of wood welding frequency on wood constituents chemical modifications. *J. Adhes. Sci. Technol.* **2009**, *23*, 1271–1279. [CrossRef]
50. Yang, H.; Wang, N.; Meng, X.; Zhu, X.; Gao, Y. Study on process parameters and mechanism of bamboo dowel rotation welding. *J. Beijing For. Univ.* **2022**, *44*, 141–150.
51. Wu, Z.; Deng, X.; Li, L.; Xi, X.; Tian, M.; Yu, L.; Zhang, B. Effects of heat treatment on interfacial properties of Pinus Massoniana wood. *Coatings* **2021**, *11*, 543. [CrossRef]
52. Lu, J.; Ding, T.; Shi, J.; Du, J. Effect of heating rate on microstructure and selected physical and mechanical properties of heat-treated Mongolian oak wood. *J. For. Eng.* **2023**, *8*, 76–83.
53. Guo, Z.; He, W.; Yuan, X.; Li, W.; Hu, G.; Wang, R.; Chen, J.; Li, X. Effect of high-temperature heat-treatment on the mould resistance of moso bamboo. *J. For. Eng.* **2023**, *8*, 32–38.